Desalination and Water Treatment
www.deswater.com

doi: 10.5004/dwt.2021.27896

244 (2021) 212–225
December

Synthesis and application of maghemite nanoparticles for water treatment: response surface method

Arfa Iqbal[a,*], Muhammad Irfan Jalees[a], Muhammad Umar Farooq[a], Emre Cevik[b], Nuhu Dalhat Mu'azu[c]

[a]*Institute of Environmental Engineering and Research, University of Engineering and Technology, P.O. Box: 54890, Lahore, Pakistan, Tel. +923434033405; email: arfa.libra@gmail.com (A. Iqbal), Tel. +923004607365; email:, jalees@uet.edu.pk (M.I. Jalees), Tel. +923154168928; email: umarfarooq@uet.edu.pk (M.U. Farooq)*
[b]*Department of Biophysics, Institute for Medical Research and Consultations, Imam Abdulrahman Bin Faisal University, P.O. Box: 1982, 31441, Dammam, Saudi Arabia, Tel. +966559322631; email: ecevik@iau.edu.sa*
[c]*Department of Environmental Engineering, College of Engineering, Imam Abdulrahman Bin Faisal University, P.O. Box: 1982, 31451, Dammam, Saudi Arabia, Tel. +966507532689; email: nmdalhat@iau.edu.sa*

Received 4 June 2021; Accepted 12 October 2021

ABSTRACT

The current study aimed at exploring potential use of maghemite nanoparticles (MNPs) synthesized via facile co-precipitation method as an adsorbent for effective water treatment. Batch adsorption studies were performed using Box–Behnken experimental design under response surface methodology to determine the effects of pH, adsorbent dose, and contact time and their interactive relationship during the adsorption process. Six water quality parameters including two physical parameters [turbidity, total dissolved solids (TDS)], one chemical parameter [chemical oxygen demand (COD)] and three heavy metals (cadmium, lead, and chromium) were selected for this study. Physicochemical properties of MNPs indicated the excellent properties of MNPs as good adsorbent. The optimized operating conditions (pH: 7, adsorbent dose: 0.75 g, and contact time: 40 min) yielded following maximum removal efficiencies for selected parameters: (89% for turbidity, 56% for TDS, 67% for COD, 79% for cadmium, 81.2% for lead, and 95.6% for chromium). Coefficient of determination (R^2) depicted a good fit between experimental and predicted values whereas larger F and smaller p-values (<0.05) of all responses indicate the higher significance of mathematical model. This study demonstrated the suitability of employing MNPs as efficient adsorbent with high potentials for the removal of multiple pollutants present in water.

Keywords: Batch adsorption; Characterization; Maghemite nanoparticles; Response surface methodology; Water quality parameters

1. Introduction

Water is considered as the core of sustainable development but unfortunately drinking water is becoming scarce day by day [1,2]. One of the sustainable development goals of United Nations is to guarantee the provision of safe drinking water to everyone by the year 2030 [3]. Although, globally groundwater contribution is less as compared to surface water but its exceptional advantages such as less capital investment, approachability, and reliability surpass the volumetric access of surface water [4]. In developing countries, many rural and urban areas meet their drinking water demands through groundwater [5–7]. Consequently, it is getting expensive and poor in quality with time due to decreasing water tables and increasing salt contents. Therefore, it has become inappropriate to utilize groundwater sources for meeting drinking water demands and hence,

* Corresponding author.

it has also become very important to pay due consideration to consumption of surface water sources to meet drinking water requirements [8]. However, surface water sources are heavily polluted owing to the existence of various types of contaminants coming from point and non-point sources of pollution, that is, anions [9], cations [10], organics [11], and microbes [12]. Presence of these pollutants makes it difficult to consume surface water for drinking purpose and unfortunately in many rural areas of developing countries, people are forced to use surface water for drinking to save treatment costs. [13]. Although, a variety of water treatment technologies have been developed, that is, ion exchange processes, advanced oxidation processes [14], coagulation [13], adsorption [15], biological treatment methods [16], and various membrane technologies [17], yet these technologies possess a wide range of drawbacks including certain health issues [18], production of large sludge volumes [19], very high treatment costs [20] and fouling issues in membranes [21]. Among all these methods, adsorption is considered as the most potential method towards advanced treatment of multiple contaminants present in water, due to its simple design [22], cost effectiveness [23], user friendliness [24], and high performance [25]. In recent years, a wide range of traditional potential adsorbents have been explored for the removal of different contaminants from water such as activated carbon [26], agricultural residues (rice husk, fruit peels, straw, and bagasse ash) [27] and a variety of industrial wastes (red mud, fly ash, and sludge) [28]. However, such materials have certain disadvantages like difficulty in processing [29] and selective removal of pollutants along with production of by-products [30].

All aspects clearly reflect the urgent need to bring advancement in water treatment technology featured with high efficiency and economical aspects for the removal of pollutants from surface water, especially in rural communities. Development of nanoparticles-based adsorbents for water treatment has been investigated during past few years [31–34]. Such materials have proven to be very attractive alternatives to conventional adsorbents due to exceptional adsorption capacity, enhanced reactivity, and excellent ability to remove various ionic, cationic, organic, inorganic, and microbial impurities from water [35–38]. Various nanosized metal oxides (ZnO, TiO_2, CeO_2, MnO_2, etc.) [32,39–44] for the elimination of toxic heavy metals from water have been investigated. Developing countries need to explore more in the field of nanotechnology to synthesize potential and low-cost nanoparticles-based adsorbents for surface water purification in order to successfully tackle the issues relevant to drinking water.

Considering the above aspects, we synthesized maghemite nanoparticles (MNPs) by a facile co precipitation method and enhanced the scope of our research by considering the removal of various major water pollutants consisting of physical and chemical parameters of water as well as heavy metals for the study instead of taking a single pollutant into account. In addition, optimization of adsorbent conditions was performed by applying Box–Behnken experimental design under response surface methodology (RSM) using Minitab software version 19, in order to achieve maximized removal efficiencies for all pollutants and for the modelling of adsorption process.

2. Materials and methods

2.1. Materials

All the chemicals and reagents used for experimentation were of analytical grade. Salts selected for the synthesis of MNPs include ferric chloride hexa-hydrated ($FeCl_3·6H_2O$) and ferrous sulfate hepta-hydrated ($FeSO_4·7H_2O$) that were obtained from Riedel-de-Haen and BDH Laboratories, UAE. For pH adjustment during synthesis process, 0.1 N NaOH and H_2SO_4 were used and obtained from BDH Laboratories, UAE. For preparation of synthetic water sample, alum ($Al_2SO_4)_3·16H_2O$, cadmium chloride ($CdCl_2·2\frac{1}{2}H_2O$), lead nitrate ($Pb(NO_3)_2$, barium chloride ($BaCl_2·2H_2O$), nickel nitrate ($NiNO_3·6H_2O$), copper sulfate ($CuSO_4·5H_2O$), chromium nitrate ($Cr(NO_3)_3·9H_2O$), sodium nitrate ($NaNO_3$), boric acid (H_3BO_3), sodium fluoride (NaF), potassium permanganate ($KMnO_4$), zinc chloride ($ZnCl_2$), calcium chloride ($CaCl_2·2H_2O$), sodium chloride (NaCl), and magnesium sulfate ($MgSO_4·7H_2O$) were used and purchased from Sigma-Aldrich, UAE. All solutions were prepared in deionized water using Thermo Scientific Deionized E-Pure Apparatus.

2.2. Preparation of MNPs

MNPs were prepared using co-precipitation method [45]. 6 M solution of an alkali (NaOH, 6 mol) solution was introduced drop by drop into a 500 mL solution of $FeCl_3·6H_2O$ (0.5 M) and $FeSO_4·7H_2O$ (0.25 M). The process was conducted at ambient temperature whereas pH maintained was 7.6 keeping constant stirring. The resulting precipitates were centrifuged and dried at 60°C for 18 h. The prepared material was thoroughly washed with deionized water to remove any excess sodium, if present. Afterwards, the precipitates were placed in oven for drying at 150°C for a period of 6 h and subsequently crushed to obtain fine powder. The resulting precipitates were nano-sized having magnetic properties. Characterization of MNPs was performed using Fourier transform infrared (FTIR; JASCO FT/IR-4100), X-ray diffraction (XRD; Philips PANalytical X'Pert), particle size analyzer (Litesizer 500), Brunauer–Emmett–Teller (BET; Nova Station A quantachrome surface area analyzer), scanning electron microscopy (SEM; Nova NanoSEM), and energy dispersive X-ray analysis (EDX; EDAX APEX).

2.3. Preparation of synthetic water sample

To prepare synthetic water sample, raw surface water sample (RSWS) was collected from Ravi Siphon, Lahore, Pakistan, and taken to the water and wastewater analysis laboratory, IEER, UET, Lahore, for its water quality analysis. All necessary water quality parameters (physical, chemical, and bacteriological) provided by World Health Organization (WHO) were analyzed according to the procedures mentioned in Standard Methods for the Examination of Water and Wastewater (22nd Edition) [46]. Salient physical, chemical, and bacteriological features of RSWS are presented in Table 1. After characterization of RSWS, synthetic water sample was artificially prepared by adding all contaminants (present in RSWS) into deionized water to keep the quality of synthetic water sample comparable with original surface water sample.

Table 1
Physical, chemical, and bacteriological characteristics of raw surface water sample

Sr. no.	Parameters	Method no.	Values	WHO guidelines
1	Color		7 TCU	<15 TCU
2	Taste		Non-Objectionable	Non-objectionable
3	Odor		Non-Objectionable	Non-objectionable
4	pH	4500-H^+ B	7.4	6.5 -8.5
5	TDS	2450 C	1,253 mg L^{-1}	<1,000 mg L^{-1}
6	Turbidity	2130 B	333 NTU	<5 NTU
7	Total hardness	2340 C	123 mg L^{-1}	–
8	Aluminum	3500-Al B	0.457 mg L^{-1}	0.2 mg L^{-1}
9	Antimony	3500-Sb B	BDL	0.02 mg L^{-1}
10	Arsenic	3500-As A	BDL	0.01 mg L^{-1}
11	Barium	3500-Ba B	0.993 mg L^{-1}	0.7 mg L^{-1}
12	Boron	3500-B B	0.104 mg L^{-1}	0.3 mg L^{-1}
13	Cadmium	3500-Cd B	1.118 mg L^{-1}	0.003 mg L^{-1}
14	Chlorides	4500-Cl^- C	225 mg L^{-1}	250 mg L^{-1}
15	Chromium	3500-Cr B	0.515 mg L^{-1}	0.05 mg L^{-1}
16	Copper	3500-Cu B	80.34 mg L^{-1}	2 mg L^{-1}
17	Cyanide		BDL	0.07 mg L^{-1}
18	Fluoride		0.2 mg L^{-1}	1.5 mg L^{-1}
19	Lead	3500-Pb B	0.895 mg L^{-1}	0.01 mg L^{-1}
20	Manganese	3500-Mn B	0.080 mg L^{-1}	0.5 mg L^{-1}
21	Mercury	3500-Hg A	BDL	0.001 mg L^{-1}
22	Nickel	3500-Ni B	2.813 mg L^{-1}	0.02 mg L^{-1}
23	Nitrate	4500-NO_3^- A	146.44 mg L^{-1}	50 mg L^{-1}
24	Nitrite	4500-NO_2^- A	108.68 mg L^{-1}	3 mg L^{-1}
25	Selenium	3500-Se B	BDL	0.01 mg L^{-1}
26	Zinc	3500-Zn B	0.026 mg L^{-1}	3 mg L^{-1}
27	*E. coli*		300 MPN/100 mL	0 MPN/100 mL
28	Fecal coliform	9221 C	1600 MPN/100 mL	0 MPN/100 mL
29	EC	2510 A	212 μS cm^{-1}	400 μS cm^{-1}
30	Sulftes	4500-SO_4^{-2} E	115 mg L^{-1}	250 mg L^{-1}
31	Alkalinity	2320 B	110.5 mg L^{-1}	–
32	Calcium	3500-Ca B	70 mg L^{-1}	75 mg L^{-1}
33	Magnesium	3500-Mg B	76 mg L^{-1}	50 mg L^{-1}
34	TOC		84 mg L^{-1}	Typical value (SMWW): 25 mg L^{-1}

This is to ensure that characteristics of the treated water used throughout the study is consistent.

2.4. Batch adsorption studies

Water treatment using MNPs was studied using batch adsorption experiments, at room temperature (25°C). For each experimental run, appropriate nanoparticles dosages were introduced to 250 mL of synthetic water sample, at a constant speed. Acidic (HCl, 0.1 N) and basic solutions (NaOH, 0.1 N) were applied for monitoring of initial pH of the solution. At the end of each experimental run, the solid phase was removed. The percentage removal of water contaminants was determined by Eq. (1):

$$\mathrm{RE}\left(\%\right)=\frac{C_0-C_e}{C_0}\times 100 \tag{1}$$

where C_0 and C_e are the initial and equilibrium concentrations of contaminants in a solution of mg L^{-1}, respectively. In order to evaluate the performance of MNPs against water treatment, a total of six water quality parameters including two physical parameters (turbidity, total dissolved solids (TDS)), one chemical parameter, that is, chemical oxygen demand (COD) and three heavy metals such as Cd, Pb, and Cr, were selected as the response of the process. All parameters were analyzed using experimental procedures provided by Standard Methods for the Examination of Water and Wastewater (22nd ed.) [46]. Turbidity was measured using turbidimeter (2130 B. Nephelometric Method) and TDS were estimated through 2540 C. TDS Dried at 180°C whereas for COD, 5220 C. Closed Reflux, Titrimetric Method was used, and removal of heavy metals was analyzed by using 3111 B. metals by flame atomic absorption spectrometry.

2.5. RSM modeling, evaluation, and optimization of operating parameters

A software Minitab 19 was used for the modeling, evaluation, and optimization of operating parameters of the process. A three (3) levels and three (3) factors Box–Behnken experimental design (BBD) under RSM was employed to evaluate the dependency of adsorption process on the operational variables, that is, pH (X_1) (4–8), adsorbent dose (X_2) (0.25–0.75 g), and contact time (X_3) (15–45 min). The experimental range and the levels of independent variables are presented in Table 2. Each process variable consisted of three levels, that is, low (–1), middle (0), and high (+1) against the six (6) investigated responses (Y_1–Y_6).

The generalized RSM fitted model was a second order polynomial equation which composed of all linear, square, and linear-by-linear interactions terms as described in Eq. (2):

$$Y = b_0 + b_1x_1 + b_2x_2 + b_3x_3 + b_{12}x_1x_2 + b_{13}x_1x_3 + b_{23}x_2x_3 + b_{11}x_{12} + b_{22}x_{22} + b_{33}x_{32} \quad (2)$$

where Y is depicting a response (percentage removal of contaminant removed) and all under studied water quality parameters including two physical parameters (turbidity, TDS), one chemical parameter, that is, COD and three heavy metals such as Cd, Pb, and Cr are designated as Y_1–Y_6, respectively; b_0 is a constant; b_1, b_2, and b_3 are linear coefficient; b_{11}, b_{22}, and b_{33} are quadratic coefficient; b_{12}, b_{13}, and b_{23} are coefficient of interaction between independent variables. Analysis of variance (ANOVA) and coefficient of regression (R^2) were used to evaluate the goodness of fit of the model.

3. Results and discussions

3.1. Characterization of MNPs

FTIR analysis of MNPs is presented in Fig. 1a. Wave numbers (889.41, 890.57, 793.61, 789.76 cm^{-1}, 532.56, 488.49, 455.57, and 416.70 cm^{-1}) correspond to the Fe-OH vibration in the sample [47,48]. These peaks indicate presence of pure MNPs in the sample. The infrared band at 1,625.57 cm^{-1} in the FTIR spectra are due to the surface OH group vibrations. Particle size analysis confirmed that the size of these nanoparticles was ranged between 800 and 1,800 μm with unimodal approach (Fig. 1b). XRD characterization (Fig. 1c) confirms the crystallinity of MNPs. The characteristic diffraction peaks at 26°, 43°, and 53° indicate the presence of Fe-O structure [49,50]. BET results suggested considerably high surface area (70.412 $m^2\ g^{-1}$) for nano scale particles (Table 3).

Table 2
Experimental range with Level of independent variables

Factors range and levels (Coded)	–1	0	1
pH: X_1	4	6	8
Adsorbent dose: X_2 (mg L^{-1})	0.25	0.5	0.75
Contact time: X_3 (min)	10	35	60

The SEM images of obtained magnetic nanoparticles are presented in Figs. 2a and b. The MNPs nanoparticles were found almost spherical or ellipsoidal having a mean diameter of 21.40 nm [51]. Meanwhile, the EDX patterns (Figs. 2c and d) used to analyze the elemental composition indicate the presence of iron and oxygen in the sample. The peaks observed at 0.4, 6.2, and 6.5 keV are indicating the binding energies of Fe, along with the peak of oxygen at 0.3 keV [52]. Hence, the EDX analysis verifies the predominant existence of both iron and oxygen in synthesized iron nanoparticles.

3.2. Developed RSM models and influence of operational conditions on responses

The BBD design matrix under RSM with coded and original values along with experimental and predicted results of all 15 experimental runs against each contaminant (response) including physical parameters (turbidity and TDS), a chemical parameter (COD) and heavy metals (Cd, Pb, and Cr) have been presented in Table 4. All laboratory tests were performed in triplicates to verify the results. Table 4 clearly depicts that all experimental and predicted values are very close to each other. The obtained turbidity and TDS removal efficiencies ranged 78%–94% and 49%–71.7%, respectively, whereas, COD removal efficiency ranged between 40% and 94%. The removal efficiencies for heavy metals were found to be in following ranges; 24%–96% for Cd, 27%–100% for Pb, and 11%–100% for Cr, respectively. Removal efficiencies of all under studied contaminants were also compared with the results obtained from literature relevant to employing various conventional and nanoadsorbents for the removal of contaminants (Table S1). A variety of literature related to individual nanoparticles, nanocomposites and biosorbents for the removal of under studied contaminants is available, however MNPs have been found to be better than the literature values which clearly depicts that MNPs have comparatively good potential toward removal of multiple contaminants simultaneously.

The regression equations in Eqs. (3)–(8) of data analysis have been generated by BBD for each response, in terms of coded investigated operational parameters. These equations support the proper concepts behind the effects of factors/parameters and their interaction with the respective response. They also imply that the factors that have more pronounced effect on a given response possess higher absolute coefficient values. Moreover, the coefficients with independent variables along with their respective signs indicate the relative effect of each variable against a respective response.

Eq. (3) presents the quadratic model for the response (Y_1), turbidity. The order of most significant parameter to the least is pH (4.813) > adsorbent dose (3.500) > contact time (0.937). The positive sign with the parameters evidently indicates that as the pH increased, turbidity removal efficiency was also increased. At low pH, positively charged MNPs, M^+ ions, attracted negatively charged pollutant particles whereas, at higher values of pH, increased rate of adsorption phenomenon was observed which might be due to the competition between H^+ ions and M^+ ions [53]. Another reason may be due to magnetic aggregation and weighting effects [54]. The coefficient of determination (R^2) of model

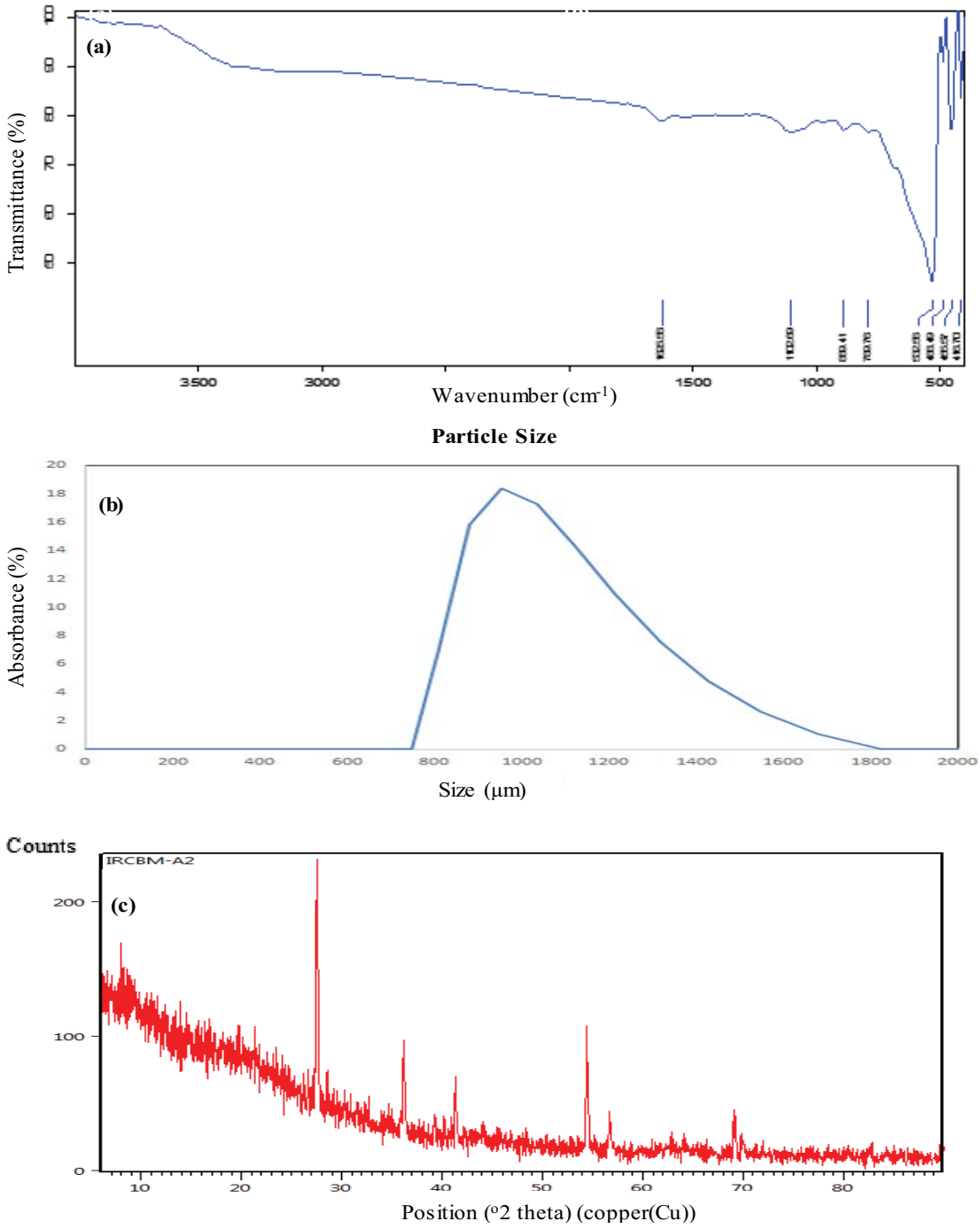

Fig. 1. (a) FTIR analysis, (b) particle size analysis, and (c) XRD analysis of MNPs.

Table 3
BET results for prepared maghemite nanoparticles (MNPs)

	Surface area	Pore volume	Pore diameter
MNPs	70.412 $m^2\ g^{-1}$	0.0315 $cm^3\ g^{-1}$	3.181 nm

was 99.27% indicating a good fit between experimental and predicted data points (Fig. 3a). In addition, it indicates that 99.27% of the variations for the turbidity removal through adsorption process are explained by independent variables and only 0.73% variations are not explained by model:

$$Y_1 = \text{Response}\left(\text{Turbidity}\right) = 78.667 + 4.813X_1 + 3.500X_2 + 0.937X_3 + 5.229X_1X_1 + 3.104X_2X_2 + 3.729X_3X_3 - 1.5X_1X_2 - 0.625X_1X_3 + 1.500X_2X_3 \quad (3)$$

Eq. (4) shows the quadratic model for the response, TDS, and the order of most significant parameter to the

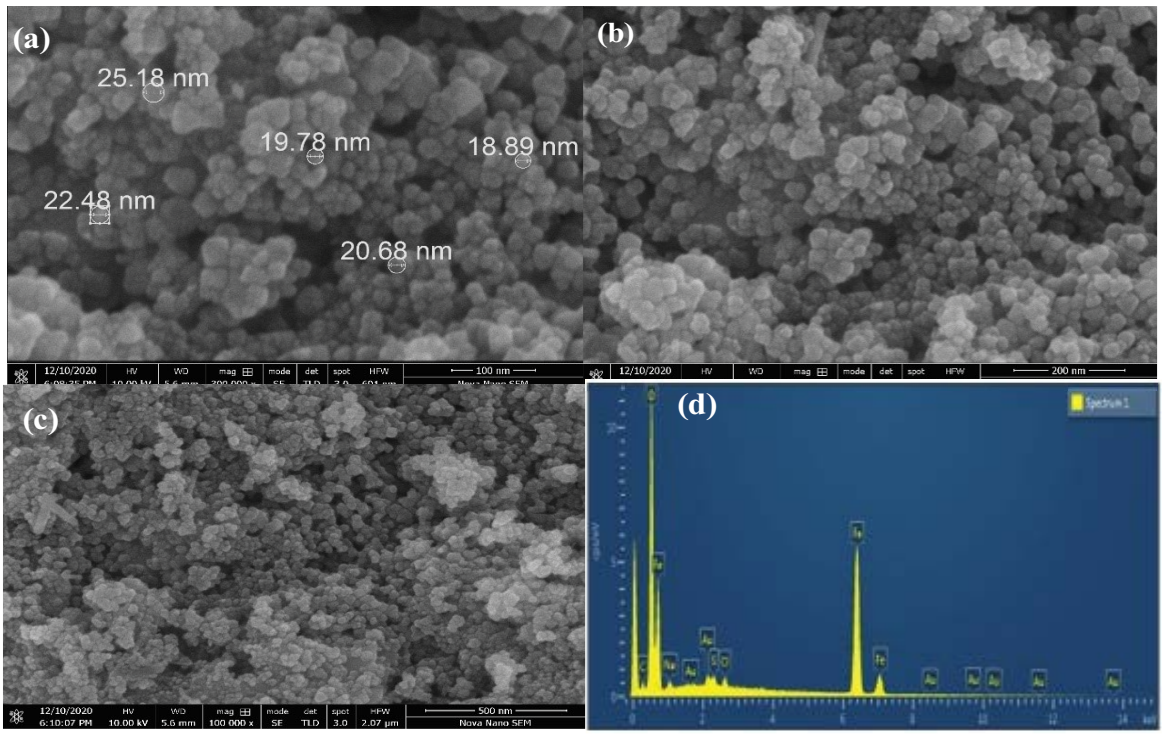

Fig. 2. SEM (a and b) and EDX analysis (c and d) of MNPs.

Table 4
Box–Behnken design (BBD) matrix of real and coded values accompanying experimental and predicted data for removal efficiency (%) of various contaminants by MNPs

Run	X_1	X_2	X_3	Y_1 = Turbidity (NTU)		Y_2 = TDS (mg L^{-1})		Y_3 = COD (mg L^{-1})		Y_4 = Cd (mg L^{-1})		Y_5 = Pb (mg L^{-1})		Y_6 = Cr (mg L^{-1})	
				Exp.	Pred.	Exp.	Pred.	Exp	Pred.	Exp.	Pred.	Exp.	Pred.	Exp.	Pred.
1	–1	–1	0	77	77.9	61	61.6	40	38.1	93	91.6	40	37.5	12	14.6
2	+1	–1	0	89	89.8	72	71.6	52	50.9	24	23.9	90	91.7	12	13.1
3	–1	+1	0	88	87.9	66	66.4	54	55.1	38	38.1	99.2	98.2	11	9.8
4	+1	+1	0	94	93.9	52	51.4	50	51.9	90	91.4	88	90.5	91	88.4
5	–1	0	–1	81	81.3	50	48.8	41	42.8	69	69.8	80	83.3	58	60.1
6	+1	0	–1	92.5	92.1	55	54.8	40	41	85	84.5	99	98.9	95	98.6
7	–1	0	+1	84	84.4	52	52.1	70	69	88	88.5	57	57.8	60	56.4
8	+1	0	+1	93	92.8	40	41.1	82	80.3	60	59.3	92	88.6	97	94.9
9	0	–1	–1	83	82.6	62	62.5	52	52.1	60	60.6	35	34.1	78	73.3
10	0	+1	–1	86	86.6	56	56.8	64	61.1	96	95.1	78	76.3	91	90
11	0	–1	+1	82	81.4	60	59.2	82	84.9	84	84.9	27	28.6	50	51
12	0	+1	+1	91	91.4	50	49.5	94	93.9	65	64.4	45	45.8	100	99.2
13	0	0	0	78	78.7	62	61.3	59	59	69	72.2	94	95.7	96	94.7
14	0	0	0	79	78.7	62	61.3	58	59	72.5	72.2	100	95.7	92	94.7
15	0	0	0	79	78.7	60	61.3	60	59	75	72.2	93	95.7	92	94

least is adsorbent dose (3.875) > contact time (2.625) > pH (1.250). Adsorbent dose has highest negative influence on TDS removal efficiency; therefore, TDS removal efficiency decreases in relation to adsorbent dose, that is, increasing adsorbent dose resulted in decreasing removal efficiency. This is due to the reason that increased adsorbent dose resulted in agglomerates formation hence decreasing the surface area available to dissolved solids [55]. R^2 of model was 99.07% which indicates a good fit between experimental and predicted values (Fig. 3b). It also indicates that

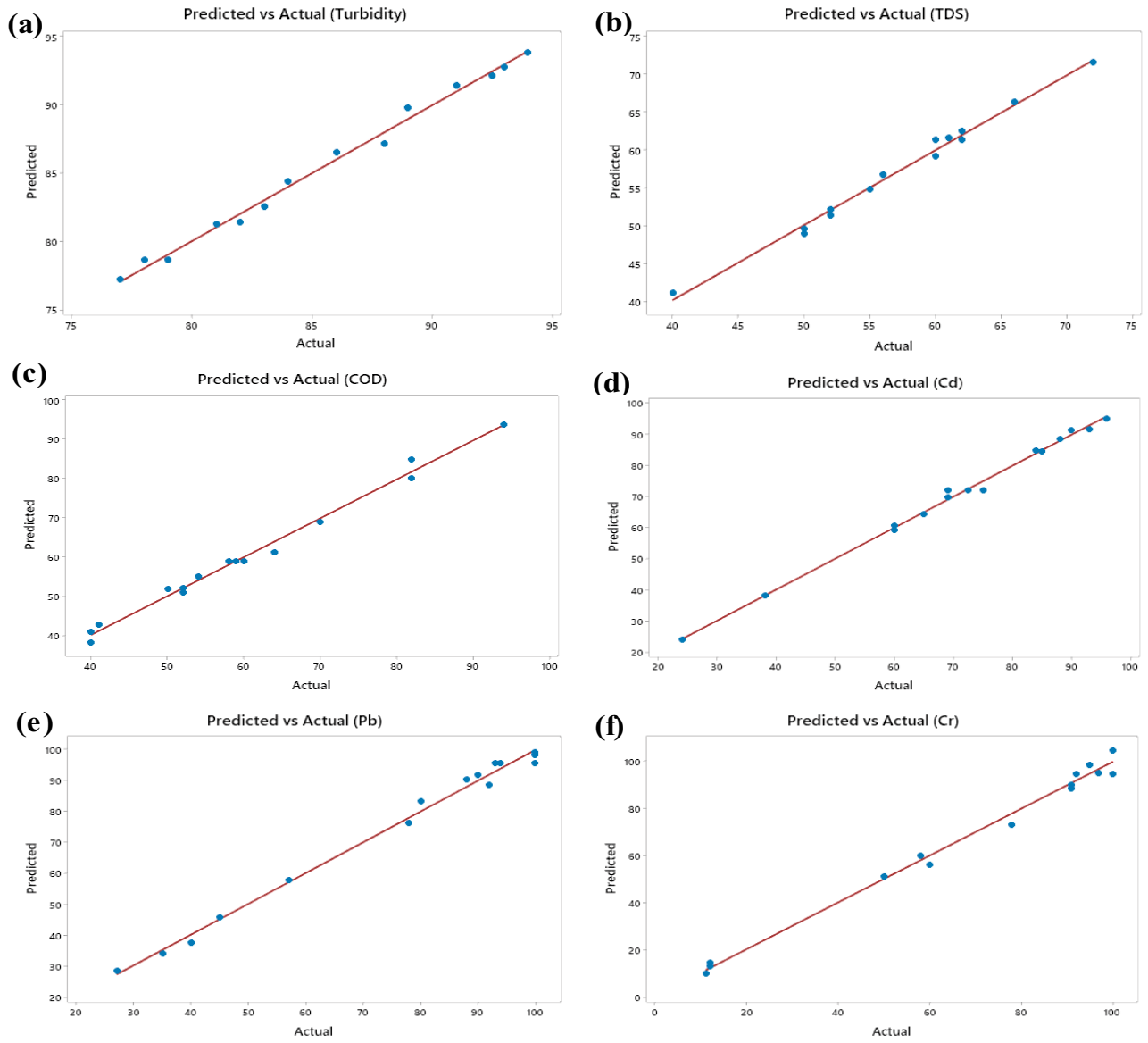

Fig. 3. Predicted vs. actual removal efficiency of (a) turbidity, (b) TDS, (c) COD, (d) Cd, (e) Pb, and (f) Cr.

99.07% of the variations for the adsorption process against TDS are explained by independent variables and only 0.93% variations have not been explained by model:

$$Y_2 = \text{Response}(\text{TDS}) = 61.333 - 1.250X_1 - 3.875X_2 - 2.625X_3 - 3.167X_1X_1 + 8.583X_2X_2 - 8.917X_3X_3 - 6.250X_1X_2 - 4.250X_1X_3 - 1.000X_2X_3 \quad (4)$$

Eq. (5) corresponds to quadratic model of response (COD) and the order of parameters is as follows; (contact time (16.375) > adsorbent dose (4.5) > pH (2.375)). All parameters have positive influence on the COD removal efficiency. Contact time has the highest positive impact on COD removal efficiency. Thus, by increasing contact time, adsorption was also increased due to availability of more vacant adsorption sites [56]. R^2 of model was 99.01% indicating that model fitted the experimental and predicted data points well (Fig. 3c) indicating only 0.99% variations, not explained.

$$Y_3 = \text{Response}(\text{COD}) = 59 + 2.375X_1 + 4.500X_2 + 16.375X_3 - 12.38X_1X_1 + 2.38X_2X_2 + 11.627X_3X_3 - 4.00X_1X_2 + 3.25X_1X_3 - 0.00X_2X_3 \quad (5)$$

Quadratic model of Cd is presented in Eq. (6) and the sequence of parameters is given as; pH (3.625) > adsorbent dose (3.5) > contact time (1.625). pH depicts highest negative effect indicating that the increase in adsorbent dose resulted in reduced Cd removal efficiency. This may be due to the fact that increased pH resulted in nucleation effect,

that is, metal and magnetic particles co attracted by electrostatic forces, hence decreasing the surface area available to heavy metal [54]. R^2 of model was 99.55% and the plot between predicted vs. actual values has been presented in Fig. 3d indicating a good fit between both sets of values. It also indicates that 99.55% of the variations for Cd removal via adsorption process are explained by independent variables and only 0.45% of the variations have not been described:

$$Y_4 = \text{Response}(\text{Cd}) = 72.17 - 3.625X_1 + 3.5X_2 - 1.625X_3 - 5.83X_1X_1 - 5.08X_2X_2 + 9.17X_3X_3 + 30.25X_1X_2 - 11.00X_1X_3 - 13.75X_2X_3 \quad (6)$$

Eq. (7) shows the quadratic model for the response, Pb and the sequence of most influential parameter to the least is adsorbent dose (14.88) > pH (11.63) > contact time (9.00). Here, adsorbent dose indicates very high positive influence on the Pb removal efficiency, that is, the increase in adsorbent dose resulted in high metal removal efficiency due to available of enough adsorption sites. However; further increasing adsorbent dose may lead to a saturation point beyond which adsorption of lead molecules will decrease with increased adsorbent dose [57]. R^2 of model was 99.19% indicating that model fitted the experimental and predicted data points well (Fig. 3e) indicating only 0.81% variations have not been explained:

$$Y_5 = \text{Response}(\text{Pb}) = 95.67 + 11.63X_1 + 14.88X_2 - 9.00X_3 + 9.92X_1X_1 - 26.08X_2X_2 - 23.33X_3X_3 - 15.50X_1X_2 + 3.75X_1X_3 - 6.25X_2X_3 \quad (7)$$

Meanwhile, Eq. (8) shows the quadratic model for the response, Cr, and the order of most significant parameter to the least is pH (19.25) > adsorbent dose (17.63) > contact time (1.87). Here, pH and adsorbent dose indicate high positive influence on the Cr removal efficiency whereas contact time has negative influence on the removal of Cr leading to saturation of active adsorbent sites available to Cr molecules [58]. R^2 of model was 99.11% which indicates a good fit between experimental and predicted values (Fig. 3f). It also indicates that only 0.89% variations are not explained by model:

$$Y_6 = \text{Response}(\text{Cr}) = 94.67 + 19.25X_1 + 17.63X_2 - 1.87X_3 - 32.71X_1X_1 - 30.46X_2X_2 + 15.54X_3X_3 + 20.00X_1X_2 - 0.0000X_1X_3 + 9.25X_2X_3 \quad (8)$$

Significance and suitability of model for all responses, that is, physical parameters, chemical parameters, and heavy metals, have been described through ANOVA results, statistically summarized in Table 5. *p*-values (with 95% confidence level) were used to evaluate the model terms. The larger Fisher (*F*) values and smaller values of *p* (<0.05) of all responses depict the higher significance of corresponding coefficients. Larger *F* values for all responses present that most of the variations can be described by the developed RSM regression equations (Y_1–Y_6). The higher adjusted and predicted R^2 values for all contaminants (under study) confirm the validation of statistical analysis through RSM for adsorption process using MNPs. All results reflect that the selected quadratic model fits appropriate in assuming the response variables for the experimental data and representing the investigated adsorptive treatment of the surface water.

3.3. Interaction effects of adsorption conditions

To analyze the effect of various factors on all responses, contour plots were plotted (Figs. 4–6). Such contour plots may be used to observe the interactive influence of the two process variables onto the response while keeping the other variable constant. Figs. 4a–f present contour plots of two responses (physical parameters), that is, (turbidity and TDS). At pH 8 and contact time (35 min), maximum turbidity and TDS removal efficiency observed was 94% with minimum adsorbent dose (0.25 g) and 72% with maximum adsorbent dose (0.75 g), respectively. Figs. 5a–c show contour plots of one response (chemical parameter), that is, COD. Maximum removal efficiency observed was 94% at pH 6 with maximum adsorbent dose (0.75 g) and contact time of 1 h. Figs. 6a–i depict contour plots of three responses (heavy metals) which include Cd, Pb, and Cr. At pH 6, Cd showed 96% removal efficiency with 0.75 g adsorbent dose in minimum contact time (10 min). Pb and Cr were removed completely from water at pH 6, however, Pb required 0.5 g adsorbent dose and 25 min, whereas, for Cr, maximum adsorbent dose (0.75 g) and contact time (45 min) were needed to get complete elimination from water.

3.4. Optimization of adsorption conditions

Response Optimizer option of software Minitab 19 was used for the prediction of optimum conditions. The objective of optimization process was to maximize the removal efficiencies of all responses within the studied operational conditions to get the best treated water, using MNPs. Fig. 7 displays the graphical representation for the removal of all contaminants from water. Hence, the optimized conditions obtained were pH = 7, adsorbent dose = 0.750 g, and contact time = 40 min. Moreover, the maximum removal efficiencies of all responses (contaminants) achieved were 89% for turbidity, 56% for TDS, 67% for COD, 79% for Cd, 81.2% for Pb, and 95.6% for Cr. The overall desirability for the solution was around 0.67 showing that within the desirable range, responses were optimized.

3.5. Conclusion

In this study, MNPs were successfully prepared by coprecipitation method and characterized by various advanced techniques. Characterization results of FTIR, XRD, particle size analysis, BET, SEM, and EDX confirm the successful formation of MNPs. Batch mode adsorption studies were conducted to examine the effectiveness of MNPs against water treatment by analyzing the removal efficiencies of selected water contaminants using Box–Behnken model under RSM. Appropriate RSM regression models were developed for predicting the removal of the investigated contaminants which satisfactorily predicted the experimental data. The high adjusted and predicted

Table 5
Analysis of variance (ANOVA) of adsorption process with all selected parameters

Source	*F*-value	*P*-value	*F*-value	*P*-value
	Turbidity		TDS	
Model	75.79	0.000	59.47	0.000
Linear	139.07	0.000	39.53	0.001
pH	266.27	0.000	7.89	0.038
Adsorbent dose	140.84	0.000	75.87	0.000
Contact time	10.10	0.025	34.82	0.002
Square	78.92	0.000	89.93	0.000
pH × pH	145.10	0.000	23.38	0.005
Adsorbent dose × adsorbent dose	51.13	0.001	48.99	0.001
Contact time × contact time	73.79	0.000	185.41	0.000
2-way interaction	9.37	0.017	48.95	0.000
pH × adsorbent dose	12.93	0.016	98.68	0.000
pH × contact time	2.25	0.194	45.63	0.001
Adsorbent dose × contact time	12.93	0.016	2.53	0.173
Error				
Lack-of-fit	2.81	0.273	1.31	0.460
Pure error				
Total				
R^2	99.27ta%		99.07%	
Adjusted R^2	99.96%		97.41%	
	COD		Cd	
Model	55.69	0.000	122.18	0.000
Linear	108.15	0.000	14.42	0.007
pH	6.22	0.055	20.28	0.006
Adsorbent dose	22.34	0.005	18.91	0.007
Contact time	295.88	0.000	4.08	0.100
Square	54.02	0.000	36.96	0.001
pH × pH	77.99	0.000	24.24	0.004
Adsorbent dose × adsorbent dose	2.87	0.151	18.41	0.008
Contact time × contact time	68.82	0.000	59.86	0.001
2-way interaction	4.89	0.060	315.14	0.000
pH × adsorbent dose	8.83	0.031	706.16	0.000
pH × contact time	5.83	0.061	93.38	0.000
Adsorbent dose × contact time	0.00	1.000	145.90	0.000
Error				
Lack-of-fit	11.42	0.082	0.28	0.836
Pure error				
Total				
R^2	99.01%		99.55%	
Adjusted R^2	97.23%		98.73%	
	Pb		Cr	
Model	67.65	0.000	61.96	0.000
Linear	74.37	0.000	64.56	0.000
pH	68.93	0.000	104.81	0.000
Adsorbent dose	112.87	0.000	87.87	0.000
Contact time	41.32	0.001	0.99	0.364
Square	103.64	0.000	98.43	0.000
pH × pH	23.15	0.005	139.66	0.000
Adsorbent dose × adsorbent dose	160.17	0.000	121.11	0.000

(Continued)

Table 5 Continued

Source	*F*-value	*P*-value	*F*-value	*P*-value
Contact time × contact time	128.18	0.000	31.53	0.002
2-way interaction	24.94	0.002	22.89	0.002
pH × adsorbent dose	61.28	0.001	56.57	0.001
pH × contact time	3.59	0.117	0.00	1.000
Adsorbent dose × contact time	9.96	0.025	12.10	0.018
Error				
Lack-of-fit	1.16	0.495	1.54	0.416
Pure error				
Total				
R^2	99.19%	99.11%		
Adjusted R^2	97.72%	97.51%		

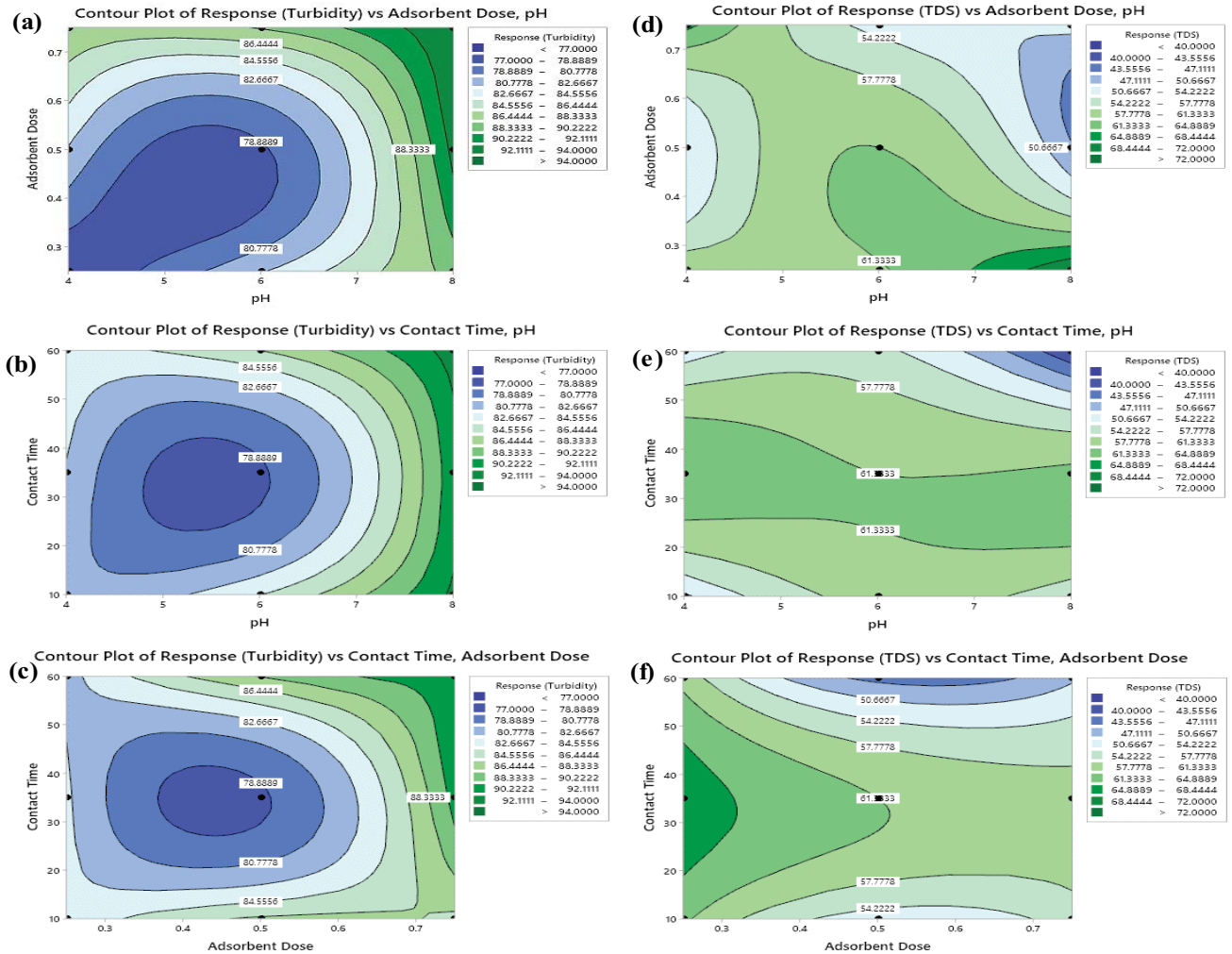

Fig. 4. Contour plots representing the effects of (a) pH and adsorbent dose-turbidity, (b) pH and contact time-turbidity, (c) adsorbent dose and contact time-turbidity, (d) pH and adsorbent dose-TDS, (e) pH and contact time-TDS, and (f) adsorbent dose and contact time-TDS.

R^2 values for contaminants confirm the validation of statistical analysis through RSM for adsorption process using MNPs. The best operating conditions obtained for the maximum removal of contaminants, that is, (turbidity (89%), TDS (56%), COD (67%), Cd (71%), Pb (81.2%), and Cr (95.6%)) were pH = 7, adsorbent dose = 0.75 g and contact time = 40 min. Based on facile nanoparticles synthesis procedure, rapid and efficient adsorption process,

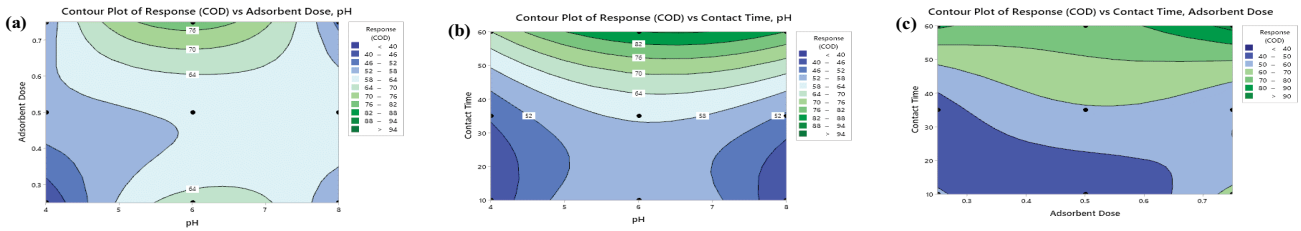

Fig. 5. Contour plots representing the effects of (a) pH and adsorbent dose-COD, (b) pH and contact time-COD, and (c) adsorbent dose and contact time-COD.

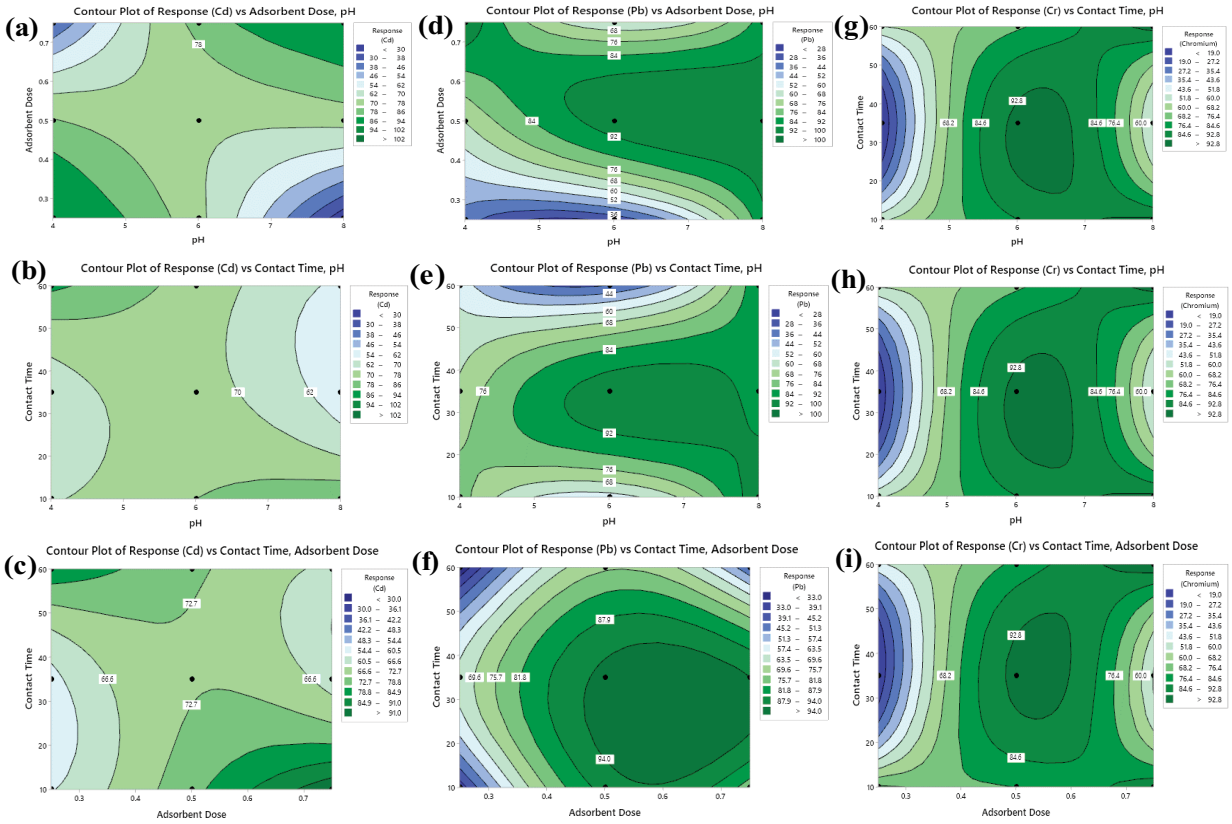

Fig. 6. Contour plots representing the effects of (a) pH and adsorbent dose-Cd, (b) pH and contact time-Cd, (c) adsorbent dose and contact time-Cd, (d) pH and adsorbent dose-Pb, (e) pH and contact time-Pb, (f) adsorbent dose and contact time-Pb, (g) pH and adsorbent dose-Cr, (h) pH and contact time-Cr, and (i) adsorbent dose and contact time-Cr.

advanced analytical characterization techniques and critical optimization studies using RSM, this study demonstrated the suitability of employing such effective MNPs as potential adsorbent for water treatment. Pilot and large-scale batch studies are required to further strengthen the present findings. Such low cost MNPs can also be further investigated for various other pollutants present in surface and ground water. In addition, MNPs can also be studied for practical solutions in wastewater treatment.

3.6. Declaration

3.6.1. Conflict of interest

Authors do not have any conflicts of interest to declare.

Funding

Authors are thankful for the provision of financial assistance by University of Engineering and Technology, Lahore, Pakistan, throughout the completion of research. Authors are also highly obliged to Higher Education Commission (HEC) Pakistan for providing research funding (PIN No: 518-86785-2Eg5-018) for this study.

Use of code

No code is used in this study.

Data availability

Data can be available on request.

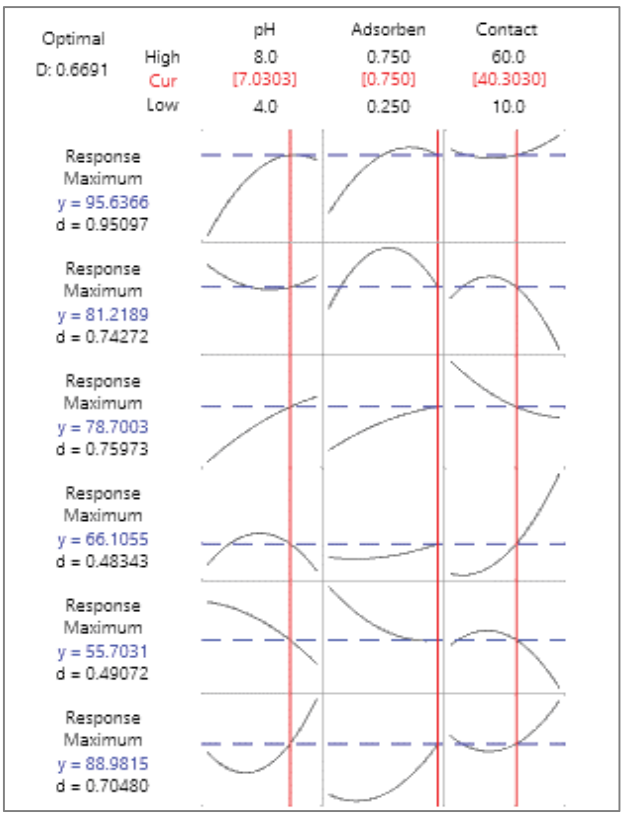

Fig. 7. Response optimization for all responses.

Symbols

C_0	—	Initial concentrations of contaminants in a solution, mg L^{-1}
C_e	—	Equilibrium concentrations of contaminants in a solution, mg L^{-1}
Y	—	Percentage removal of contaminant removed, %
b_1, b_2, and b_3	—	Linear coefficient
b_{11}, b_{22}, and b_{33}	—	Quadratic coefficient
b_{12}, b_{13}, and b_{23}	—	Coefficient of interaction between independent variables
Y_1	—	Turbidity, NTU
Y_2	—	Total dissolved solids, mg L^{-1}
Y_3	—	Chemical oxygen demand, mg L^{-1}
Y_4	—	Cadmium, mg L^{-1}
Y_5	—	Lead, mg L^{-1}
Y_6	—	Chromium, mg L^{-1}
X_1	—	pH
X_2	—	Adsorbent dose, mg L^{-1}
X_3	—	Contact time, min

References

[1] C. Tortajada, P. Rensburg, Drink More Recycled Wastewater, NPG, 2020.

[2] I.R. Orimoloye, J.A. Belle, A.O. Olusola, E.T. Busayo, O.O. Ololade, Spatial assessment of drought disasters, vulnerability, severity and water shortages: a potential drought disaster mitigation strategy, Nat. Hazards, 105 (2021) 2735–2754.

[3] L. Karthik, A.V. Kirthi, S. Ranjan, V.M. Srinivasan, Biological Synthesis of Nanoparticles and Their Applications, CRC Press, New York, 2020.

[4] A. Iqbal, G. Hussain, S. Haydar, N. Zahara, Use of new local plant-based coagulants for turbid water treatment, Int. J. Environ. Sci. Technol., 16 (2019) 6167–6174.

[5] I.E. de Graaf, R.L. Beek, T. Gleeson, N. Moosdorf, O. Schmitz, E.H. Sutanudjaja, M.F.P. Bierkens, A global-scale two-layer transient groundwater model: development and application to groundwater depletion, Adv. Water Resour., 102 (2017) 53–67.

[6] N. Ferrer, A. Folch, G. Maso, S. Sanchez, X.S. Vila, What are the main factors influencing the presence of faecal bacteria pollution in groundwater systems in developing countries?, J. Contam. Hydrol., 228 (2020) 103556, doi: 10.1016/j.jconhyd.2019.103556.

[7] V. Masindi, S. Foteinis, Groundwater contamination in sub-Saharan Africa: implications for groundwater protection in developing countries, Cleaner Eng. Technol., 2 (2021) 100038, doi: 10.1016/j.clet.2020.100038.

[8] A. Iqbal, N. Zahara, Coagulation efficiency comparison of natural and its blended coagulant with alum in water treatment, Desal. Water Treat., 109 (2018) 188–192.

[9] J. Wang, S. Wang, Effect of inorganic anions on the performance of advanced oxidation processes for degradation of organic contaminants, Chem. Eng. J., 411 (2021) 128392, doi: 10.1016/j.cej.2020.128392.

[10] N.D. Shooto, E.B. Naidoo, M. Maubane, Sorption studies of toxic cations on ginger root adsorbent, J. Ind. Eng. Chem., 76 (2019) 133–140.

[11] R.J.C. Go, H.-L. Yang, C.-C. Kan, D.C. Ong, S.G. Segura, M.D.G. Luna, Natural organic matter removal from raw surface water: benchmarking performance of chemical coagulants through excitation-emission fluorescence matrix spectroscopy analysis, Water, 13 (2021) 146, doi: 10.3390/w13020146.

[12] L. Wang, J. Zhang, H. Li, H. Yang, C. Peng, Z. Peng, L. Lu, Shift in the microbial community composition of surface water and sediment along an urban river, Sci. Total Environ., 627 (2018) 600–612.

[13] K. Khan, Y. Lu, M.A. Saeed, H. Bilal, H. Sher, H. Khan, J. Ali, P. Wang, H. Uwizeyimana, Y. Baninla, Q. Li, Z. Liu, J. Nawab, Y. Zhou, C. Su, R. Liang, Prevalent fecal contamination in drinking water resources and potential health risks in Swat, Pakistan, J. Environ. Sci., 72 (2018) 1–12.

[14] G.-R. Chen, Y.-R. Chang, X. Liu, T. Kawamoto, H. Tanaka, D. Parajuli, T. Kawasaki, Y. Kawatsu, T. Kobayashi, M.-L. Chen, Y.-K Lo, Z. Lei, D.-J. Lee, Cesium removal from drinking water using Prussian blue adsorption followed by anion exchange process, Sep. Purif. Technol., 172 (2017) 147–151.

[15] J. Gjipalaj, I. Alessandri, Easy recovery, mechanical stability, enhanced adsorption capacity and recyclability of alginate-based TiO_2 macrobead photocatalysts for water treatment, J. Environ. Chem. Eng., 5 (2017) 1763–1770.

[16] M. Bourgin, B. Beck, M. Boehler, E. Borowska, J. Fleiner, E. Salhi, R. Teichler, U. Gunten, H. Siegrist, C.S. McArdell, Evaluation of a full-scale wastewater treatment plant upgraded with ozonation and biological post-treatments: abatement of micropollutants, formation of transformation products and oxidation by-products, Water Res., 129 (2018) 486–498.

[17] C.K. Bolat, Investigation of Parameters Affecting Morphology of Microfiltration and Ultrafiltration Membranes Fabricated via Phase Separation Microfabrication, Middle East Technical University, 2017.

[18] S. Boulaadjoul, H. Zemmouri, Z. Bendjama, N. Drouiche, A novel use of *Moringa oleifera* seed powder in enhancing the primary treatment of paper mill effluent, Chemosphere, 206 (2018) 142–149.

[19] J.C. Brown, C.T. Cleveland, Biological Two-Stage Contaminated Water Treatment System, Google Patents, 2018.

[20] P. Jelonek, E. Neczaj, The use of advanced oxidation processes (AOP) for the treatment of landfill leachate, Environ. Prot. Eng., 15 (2012) 203–217.

[21] T. Nguyen, F. Roddick, L. Fan, Biofouling of water treatment membranes: a review of the underlying causes, monitoring techniques and control measures, Membranes, 2 (2012) 804–840.

[22] C. Didaskalou, S. Buyuktiryaki, R. Kecili, C.P. Fonte, G. Szekely, Valorisation of agricultural waste with an adsorption/nanofiltration hybrid process: from materials to sustainable process design, RSC Adv., 19 (2017) 3116–3125.
[23] R. Chakraborty, A. Asthana, A.K. Singh, B. Jain, A.B.H. Susan, Adsorption of heavy metal ions by various low-cost adsorbents: a review, Int. J. Environ. Anal. Chem., (2020) 1–38, doi: 10.1080/03067319.2020.1722811.
[24] Q. Li, M. Wang, X. Yuan, D. Li, H. Xu, L. Sun, F. Pan, D. Xia, Study on the adsorption and desorption performance of magnetic resin for Congo red, Environ. Technol., 42 (2021) 1552–1559.
[25] M. Jargalsaikhan, J. Lee, L. Jang, S. Jeong, Efficient removal of azo dye from wastewater using the non-toxic potassium ferrate oxidation–coagulation process, Appl. Sci., 11 (2021) 6825, doi: 10.3390/app11156825.
[26] D. Lu, S. Xu, W. Qiu, Y. Sun, X. Liu, J. Yang, J. Ma, Adsorption and desorption behaviors of antibiotic ciprofloxacin on functionalized spherical MCM-41 for water treatment, J. Cleaner Prod., 264 (2020) 121644, doi: 10.1016/j.jclepro.2020.121644.
[27] F.M. Mpatani, A.A. Aryee, A.N. Kani, Q. Guo, E. Dovi, L. Qu, Z. Li, R. Han, Uptake of micropollutant-bisphenol A, methylene blue and neutral red onto a novel bagasse-β-cyclodextrin polymer by adsorption process, Chemosphere, 259 (2020) 127439, doi: 10.1016/j.chemosphere.2020.127439.
[28] M.A. Tony, Zeolite-based adsorbent from alum sludge residue for textile wastewater treatment, Int. J. Environ. Sci. Technol., 17 (2020) 2485–2498.
[29] H. Zeng, Y. Yu, F. Wang, J. Zhang, D. Li, Arsenic(V) removal by granular adsorbents made from water treatment residuals materials and chitosan, Colloids Surf., A, 585 (2020) 124036, doi: 10.1016/j.colsurfa.2019.124036.
[30] H. Sadegh, G.A. Ali, Potential Applications of Nanomaterials in Wastewater Treatment: Nanoadsorbents Performance, In: Research Anthology on Synthesis, Characterization, and Applications of Nanomaterials, IGI Global, International Symposium on Nanostructured, Nanoengineered and Advanced Materials (ISNNAM 2020), South Africa, 2021, pp. 1230–1240.
[31] J. Brame, Q. Li, P.J. Alvarez, Nanotechnology-enabled water treatment and reuse: emerging opportunities and challenges for developing countries, Trends Food Sci. Technol., 22 (2011) 618–624.
[32] Y. Chen, Y. Liu, Y. Li, Y. Wu, Y. Chen, Y. Liu, J. Zhang, F. Xu, M. Li, L. Li, Synthesis, application and mechanisms of Ferro-Manganese binary oxide in water remediation: a review, Chem. Eng. J., 388 (2020) 124313, doi: 10.1016/j.cej.2020.124313.
[33] M. Sagir, M. Tahir, Role of nanocatalyst (photocatalysts) for waste water treatment, Curr. Anal. Chem.,17 (2021) 138–149.
[34] T. Sahoo, J.R. Sahu, J. Panda, M. Hembram, S.K. Sahoo, R. Sahu, Nanotechnology: An Efficient Technique of Contaminated Water Treatment, M. Kumar, D. Snow, R. Honda, S. Mukherjee, Eds., Contaminants in Drinking and Wastewater Sources, Springer, Singapore, 2021, pp. 251–270.
[35] R. Das, M.E. Ali, S. Hamid, S. Ramakrishna, Z. Chowdhury, Carbon nanotube membranes for water purification: a bright future in water desalination, Desalination, 336 (2014) 97–109.
[36] A. Ismail, S. Ajayi, A. Alausa, O. Ogundile, O. Ademosun, Antimicrobial and antibiofilm activities of green synthesized silver nanoparticles for water treatment, J. Phys. Conf. Ser., 1734 (2021) 012043.
[37] N. Shabani, A. Javadi, H.J. Malmiri, H. Mirzaie, J. Sadeghi, Potential application of iron oxide nanoparticles synthesized by co-precipitation technology as a coagulant for water treatment in settling tanks, Min. Metall Explor., 38 (2021) 269–276.
[38] S.F. Soares, T. Fernandes, T. Trindade, A.L.D. Silve, Recent advances on magnetic biosorbents and their applications for water treatment, Environ. Chem. Lett.,18 (2020) 151–164.
[39] D. Dodoo-Arhin, T. Asiedu, B.A. Tuffour, E. Nyankson, D. Obada, J.M. Mwabora, Photocatalytic degradation of Rhodamine dyes using zinc oxide nanoparticles, Mater. Today Proc., 38 (2021) 809–815.
[40] M.E. Mahmoud, G.A.A. Ibrahim, M.S. Abdelwahab, Manganese dioxide nanoparticles decorated with chitosan for effective removal of lead and lanthanum ions from water by microwave sorption technique, Mater. Sci. Eng., 267 (2021) 115091, doi: 10.1016/j.mseb.2021.115091.
[41] R. Li, W. Yang, S. Gao, J. Shang, Hydrous cerium oxides coated glass fiber for efficient and long-lasting arsenic removal from drinking water, J. Adv. Ceram., 10 (2021) 247–257.
[42] Y. Chen, H. Shi, H. Guo, C. Ling, X. Yuan, P. Li, Hydrated titanium oxide nanoparticles supported on natural rice straw for Cu(II) removal from water, Environ. Technol. Innovation, 20 (2020) 101143, doi: 10.1016/j.eti.2020.101143.
[43] N.M. El-Shafai, M. Shukry, I.M. El-Mehasseb, M. Abdelfatah, M.S. Ramadan, A. El-Shaer, M. El-Kemary, Electrochemical property, antioxidant activities, water treatment and solar cell applications of titanium dioxide–zinc oxide hybrid nanocomposite based on graphene oxide nanosheet, Mater. Sci. Eng. B, 259 (2020) 114596, doi: 10.1016/j.mseb.2020.114596.
[44] G. Yashni, A. Al-Gheethi, R. Mohamed, M.S. Hossain, A.F. Kamil, V.A. Shanmugan, Photocatalysis of xenobiotic organic compounds in greywater using zinc oxide nanoparticles: a critical review, Water Environ. J., 35 (2021) 190–217.
[45] A.A. Abubakar, M. Abdullahi, S.A. Hassan, Synthesis, characterization and application of nickel and iron nanoparticles using co-precipitation method, FRsCS, 1 (2019) 67–73.
[46] I.V. Carranzo, Standard Methods for Examination of Water and Wastewater, Anales De Hidrología Médica, Universidad Complutense de Madrid, 2012.
[47] A. Lassoued, B. Dkhil, A. Gadri, S. Ammar, Control of the shape and size of iron oxide (α-Fe_2O_3) nanoparticles synthesized through the chemical precipitation method, Results Phys., 7 (2017) 3007–3015.
[48] X. Cai, X. Yu, X. Yu, Z. Wu, S. Li, C. Yu, Synthesis of illite/iron nanoparticles and their application as an adsorbent of lead ions, Environ. Sci. Pollut. Res., 26 (2019) 29449–29459.
[49] S Saqib, M.F.H. Munis, W. Zaman, F. Ullah, S.N. Shah, A. Ayaz, M. Farooq, S. Bahadur, Synthesis, characterization and use of iron oxide nano particles for antibacterial activity, Microbiol. Res. Technol., 82 (2019) 415–420.
[50] A. Lassoued, M.S. Lassoued, B. Dkhil, S. Ammar, A. Gadri, Synthesis, structural, morphological, optical and magnetic characterization of iron oxide (α-Fe_2O_3) nanoparticles by precipitation method: effect of varying the nature of precursor, Phys. E Low Dimens. Syst. Nanostruct., 97 (2018) 328–334.
[51] M. Neamtu, C. Nadejde, V.-D. Hodoroaba, R.J. Schneider, L. Verestiuc, U. Panne, Functionalized magnetic nanoparticles: synthesis, characterization, catalytic application and assessment of toxicity, Sci. Rep., 8 (2018) 1–11.
[52] K. Nithya, A. Sathish, P.S. Kumar, T. Ramachandran, Fast kinetics and high adsorption capacity of green extract capped superparamagnetic iron oxide nanoparticles for the adsorption of Ni(II) ions, J. Ind. Eng. Chem., 59 (2018) 230–241.
[53] D.R. Samayamanthula, C. Sabarathinam, H. Bhandary, Treatment and effective utilization of greywater, Appl. Water Sci., 9 (2019) 90, doi: 10.1007/s13201-019-0966-0.
[54] S.-L. Lo, Y.-L. Wang, C.-Y. Hu, High turbidity reduction during the storm period by applied magnetic field, J. Environ. Eng. Manage., 17 (2008) 365–370.
[55] M.U. Farooq, M.I. Jalees, A. Iqbal, N. Zahara, A. Kiran, Characterization and adsorption study of biosorbents for the removal of basic cationic dye: kinetic and isotherm analysis, Desal. Water Treat., 160 (2019) 333–342.
[56] A.A. Alghamdi, A.-B. Al-Odayni, W.S. Saeed, A. Al-Kahtani, F.A. Alharthi, T. Aouak, Efficient adsorption of lead(II) from aqueous phase solutions using polypyrrole-based activated carbon, Materials, 12 (2019) 2020, doi: 10.3390/ma12122020.
[57] S.N. Abas, M. Halim, M.L. Kamal, S. Izhar, Adsorption process of heavy metals by low-cost adsorbent: a review, World Appl. Sci. J., 28 (2013) 1518–1530.
[58] L.T.M. Thy, N.H. Thuong, T.H. Tu, H.M. Nam, N.H. Hieu, M.T. Phong, Synthesis of magnetic iron oxide/graphene oxide nanocomposites for removal of cadmium ions from water, ANSN, 10 (2019) 025006, doi: 10.1088/2043-6254/ab1b79.

Supplementary information:

Table S1
Comparison of removal efficiencies achieved by MNPs for contaminants (under study) with literature data

Adsorbent material	Removal efficiency (%)	Reference
	Turbidity	
MNPs	89%	Present study
Graphene oxide	75%	[S1]
Chitosan	50.5%	[S2]
Polyaluminum chloride	66.59%	[S3]
	TDS	
MNPs	56%	Present study
Magnesium oxide nanoparticles	47.6%	[S4]
4-nonylphenol	51.32%	[S5]
Chitosan	12.87%	[S2]
	COD	
MNPs	67%	Present study
Activated carbon	60%	[S6]
Magnetite nanoparticles	42%	[S7]
Chitosan	61.2%	[S8]
	Cadmium	
MNPs	71%	Present study
Red mud	60%	[S9]
Silica gel	16%	[S10]
MnO_2 nanostructures	70%	[S11]
	Lead	
MNPs	81.2%	Present study
MWCNTs	60%	[S12]
MnO_2 nanostructures	70%	[S13]
Chitosan	70%	[S14]
	Chromium	
MNPs	95.6%	Present study
Kaolin	78%	[S15]
Graphene oxide	92%	[S16]
MWCNTs	18%	[S17]

References

[S1] A.E. Aboubaraka, E.F. Aboelfetoh, E.-Z.M. Ebeid, Coagulation effectiveness of graphene oxide for the removal of turbidity from raw surface water, Chemosphere, 181 (2017) 738–746.

[S2] A.J. Al-Manhel, A.R.S. Al-Hilphy, A.K. Niamah, Extraction of chitosan, characterisation and its use for water purification, J. Saudi Soc. Agric. Sci., 17 (2018) 186–190.

[S3] Z. Wu, X. Zhang, J. Pang, X. Zhang, J. Li, J. Li, P. Zhang, Humic acid removal from water with PAC-Al30: effect of calcium and kaolin and the action mechanisms, J. Am. Chem. Soc., 5 (2020) 16413–16420.

[S4] A. Fouda, S.E.-D. Hassan, M.A. Abdel-Rahman, M.M.S. Farag, A. Shehal-Deen, A.A. Mohamed, S.M. Alsharif, E. Saied, S.A. Moghanim, M.S. Azab, Catalytic degradation of wastewater from the textile and tannery industries by green synthesized hematite (α-Fe_2O_3) and magnesium oxide (MgO) nanoparticles, Curr. Res. Biotechnol., 3 (2021) 29–41.

[S5] M. Safari, N. Mehrdadi, M. Baghdadi, G.N. Bidhendi, Removal capability of 4-nonylphenol using new nano-adsorbents produced in sand filters of water treatment plants, Mater. Res. Express, 8 (2021) 045601, doi: 10.1088/2053-1591/abafcd

[S6] M.N. Rashed, Adsorption technique for the removal of organic pollutants from water and wastewater, Org. Pollut. Monit. Risk Treat., 7 (2013) 167–194.

[S7] P. Nanta, K. Kasemwong, W. Skolpap, Isotherm and kinetic modeling on superparamagnetic nanoparticles adsorption of polysaccharide, J. Environ. Chem. Eng., 6 (2018) 794–802.

[S8] H. Peng, C. Zou, C. Wang, W. Tang, J. Zhou, The effective removal of phenol from aqueous solution via adsorption on CS/β-CD/CTA multicomponent adsorbent and its application for COD degradation of drilling wastewater, Environ. Sci. Pollut. Res., 27 (2020) 33668–33680.

[S9] Renu, M. Agarwal, K. Singh, Heavy metal removal from wastewater using various adsorbents: a review, J. Water Reuse Desal., 7 (2017) 387–419.

[S10] L. Renugopal, K. Kow, P.L. Kiew, S.P. Yeap, H.S. Chua, C.H. Chan, R. Yusoff, Selective adsorption of copper and cadmium ions using nano-particles aligned *in silica* gel matrix, AIP Conf Proc., 2124 (2019) 020001 (1–9), doi: 10.1063/1.5117061.

[S11] R. Zhai, Y. Wan, L. Liu, X. Zhang, W. Wang, J. Liu, B. Zhang, Hierarchical MnO_2 nanostructures: synthesis and their application in water treatment, Water Sci. Technol., 65 (2012) 1054–1059.

[S12] J.-G. Yu, X.-H. Zhao, L.-Y. Yu, F.-P. Jiao, J.-H. Jiang, X.Q. Chen, Removal, recovery and enrichment of metals from aqueous solutions using carbon nanotubes, J. Radioanal. Nucl. Chem., 299 (2014) 1155–1163.

[S13] S. Mallakpour, A. Abdolmaleki, H. Tabebordbar, Production of PVC/α-MnO_2-KH550 nanocomposite films: morphology, thermal, mechanical and Pb(II) adsorption properties, Eur. Polym. J., 78 (2016) 141–152.

[S14] M. Bhatia, R.S. Babu, S.H. Sonowane, P.R. Gogate, A. Girdhar, E.R. Reddy, M. Pola, Application of nanoadsorbents for removal of lead from water, Int. J. Environ. Sci. Technol., 14 (2017) 1135–1154.

[S15] S. Mustapha, J.O. Tijani, M.M. Ndamitso, S.A. Abdulkareem, D.T. Shuaib, A.K. Mohammed, A. Sumaila, The role of kaolin and kaolin/ZnO nanoadsorbents in adsorption studies for tannery wastewater treatment, Sci. Rep., 10 (2020) 1–22.

[S16] İ. Duru, D. Ege, A.R. Kamali, Graphene oxides for removal of heavy and precious metals from wastewater, J. Mater. Sci., 51 (2016) 6097–6116.

[S17] M.A. Atieh, O.Y. Bakather, B.S. Tawabini, A.A. Bukhari, M. Khaled, M. Alharthi, M. Fettouhi, F.A. Abuilaiwi, Removal of chromium(III) from water by using modified and nonmodified carbon nanotubes, J. Nanomater., 2010 (2010) 232378 (1–9). doi: 10.1155/2010/232378.